

Hot electron transport in Ballistic Electron Emission Spectroscopy: Band structure effects and k_{\parallel} -space currents

K. REUTER^{1,2}, P. L. DE ANDRES¹, F. J. GARCIA-VIDAL³, F. FLORES³
U. HOHENESTER^{4,5} and P. KOCEVAR⁵

¹ *Instituto de Ciencia de Materiales (CSIC), Cantoblanco - E-28049 Madrid, Spain*

² *Lehrstuhl für Festkörperphysik, University of Erlangen-Nürnberg, Germany*

³ *Departamento de Física Teórica de la Materia Condensada*

Universidad Autónoma de Madrid - E-28049 Madrid, Spain

⁴ *Istituto Nazionale per la Fisica della Materia and Dipartimento di Fisica*

Università di Modena - I-41100 Modena, Italy

⁵ *Institut für Theoretische Physik, Karl-Franzens-Universität Graz*

A-8010 Graz, Austria

(received 27 April 1998; accepted in final form 8 November 1998)

PACS. 61.16Ch – Scanning probe microscopy: scanning tunneling, atomic force, scanning optical, magnetic force, etc.

PACS. 72.10Bg – General formulation of transport theory.

PACS. 73.20At – Surface states, band structure, electron density of states.

Abstract. – Using a Green’s function approach, we investigate band structure effects in the BEEM current distribution in k_{\parallel} -space. In the elastic limit, this formalism provides a “parameter free” solution of the BEEM problem. At low temperatures, and for thin metallic layers, the elastic approximation is enough to explain the experimental $I(V)$ curves at low voltages. At higher voltages inelastic effects are approximately taken into account by introducing an effective RPA-electron lifetime, much in similarity with LEED theory. For thick films, however, additional damping mechanisms are required to obtain agreement with experiment.

Ballistic Electron Emission Microscopy (BEEM), and its spectroscopic counterpart (BEES) [1], were originally designed as techniques extending the power of Scanning Tunneling Microscopy (STM) to buried interfaces, particularly of metal-semiconductor systems. The standard model describes BEEM as a convolution of three steps [2]: 1) tunneling from the tip, 2) propagation in the metallic layer and 3) transmission through the metal-semiconductor interface. This model clearly suggests the important potential of BEEM to focus in any of these steps separately. However, it is unnecessary to stress that such a deconvolution process may only be safely performed by applying for each of those steps a sufficiently elaborated theory, which should use as few adjustable parameters as possible. In the past, the lack of such a precise method to analyze the experiment has prompted several intense discussions: i) whether k_{\parallel} is conserved or not at the interface [3], ii) the origin of the observed nanometric resolution and its relation

to the tunneling injection [4], iii) the similar results obtained on Au/Si(111) and Au/Si(100) interfaces, despite their different projected conduction-band minima [5], iv) are the electrons in BEEM *ballistic* after all? [2], etc. This list of intensively debated questions in the literature is probably an indication of the limitations associated with the standard approach based on E -space Monte Carlo simulations, where processes crucial from a physical point of view are simply parametrized to give agreement with experiment. In particular, in all these Monte Carlo calculations, the energetic spectrum and the momentum distribution of the injected electrons are taken from conventional planar tunneling theory, using a free-electron approach. This assumption is probably the origin of the major limitation for the analysis of the BEEM current, as the propagation of the electrons in the metal film is strongly dependent on the metal band structure and can depart significantly from a free-electron behaviour [6]. Accordingly, the aim of this letter is to present a microscopic formalism that incorporates those band structure effects and yields the appropriate angular momentum distribution that, as shown below for the case of gold films, is drastically different from the narrow forward cone assumed in E -space Monte Carlo simulations. We shall show how most of the previous interpretations of BEEM data for Au/Si interfaces need to be modified when using the right k -space currents.

We introduce a full quantum-mechanical description of the BEEM problem based on a Keldysh Green's function method written in a Linear Combination of Atomic Orbitals (LCAO) basis. Our analysis is based on the following three-step scheme: We provide an accurate description of the initial tunneling injection (1), and the subsequent propagation of electrons through the metallic layer (2). Passing over the Schottky barrier (3) is taken into account applying energy and k_{\parallel} conservation, and matching states at the *two-dimensional* interface. In this paper the foregoing scheme is applied to the case study of a (111)-oriented gold metallic layer deposited on a (111) silicon substrate; applications to other metals (*e.g.*, CoSi₂) and other semiconductors are in progress. Perfect unrelaxed surfaces and bulk-like ideal geometries are assumed in our analysis, but it is seen from the nature of our results that a relatively small amount of disorder (*e.g.*, confined to 4-5 layers close to the interface) would not fundamentally change our conclusions.

A Green's function formalism presents the important advantage of being free of any adjustable parameter in the strictly elastic limit, where we only add an arbitrarily small positive imaginary part to the energy (η), necessary to ensure attenuation of the wave at infinity. Moreover, inelastic effects associated with the electron-electron interaction can be added incorporating a complex energy-dependent self-energy, $\eta(E)$. We shall view the self-energy as a single parameter to be adjusted to the experiment, representing an effective inelastic electron-electron mean free path producing attenuation: $\lambda_{\text{att}} \approx \frac{\sqrt{2E}}{2\eta}$. This method has been successfully adopted to different fields, like Low-Energy Electron Diffraction.

In an LCAO basis, we write the Hamiltonian as

$$\hat{H} = \hat{H}_{\text{T}} + \hat{H}_{\text{S}} + \hat{H}_{\text{I}}, \quad (1)$$

where $\hat{H}_{\text{T}} = \sum \epsilon_{\alpha} \hat{n}_{\alpha} + \sum \hat{T}_{\alpha\beta} \hat{c}_{\alpha}^{\dagger} \hat{c}_{\beta}$ defines the tip (Greek subindices), $\hat{H}_{\text{S}} = \sum \epsilon_i \hat{n}_i + \sum \hat{T}_{ij} \hat{c}_i^{\dagger} \hat{c}_j$ designates the metal substrate (Latin subindices), and $\hat{H}_{\text{I}} = \sum \hat{T}_{\alpha j} \hat{c}_{\alpha}^{\dagger} \hat{c}_j$ describes the coupling between the tip and the metal surface in terms of a hopping matrix, $\hat{T}_{\alpha j}$, expressed as a function of the different atomic orbitals in the tip and the surface by using a tight-binding formalism [7,8] (\hat{n}_{α} , $\hat{c}_{\alpha}^{\dagger}$, and \hat{c}_{α} , are number, creation and destruction operators defined in the usual way).

Since the system under investigation is out of equilibrium, a convenient way to compute

the current between two sites i and j in real space is given by Keldysh's technique [9]

$$J_{ij} = \int \text{Tr}\{\widehat{T}_{ij}(\widehat{G}_{ij}^{+-} - \widehat{G}_{ji}^{+-})\}dE. \quad (2)$$

The matrices \widehat{G}_{ji}^{+-} are non-equilibrium Keldysh Green's functions that can be calculated in terms of the standard retarded and advanced Green's functions [6, 10]. We notice that this formalism allows us to compute on the same footing the tunneling current between the tip and the sample, and the current propagating in the metal (steps 1 and 2). To this point, all our expressions are exact, and the main task is to determine how to compute the retarded and advanced Green functions, and which approximations are introduced there.

Previously [6], we have analyzed the electron propagation in real space, using a semiclassical approximation for these Green functions, and we have found important focusing effects in gold films. Now, we concentrate on calculating the full quantum-mechanical current distribution in 2D reciprocal space, using a formalism based on renormalization group techniques [11]. This k_{\parallel} -current distribution will allow us to obtain the spectral $I(V)$ characteristics. In particular, the current between two layers a and b inside the metal, at a given energy E and k_{\parallel} , can be expressed as [6, 12]

$$J_{ab}(E, k_{\parallel}) = \frac{2e}{\pi\hbar} \Re \text{Tr}\{\widehat{T}_{ab}\widehat{g}_{b1}^R\widehat{T}_{10}\widehat{\rho}_{00}\widehat{T}_{01}\widehat{g}_{1a}^A\}, \quad (3)$$

where $\widehat{g}_{b1}^{R(A)}(E, k_{\parallel})$ is the retarded (advanced) Green's function for the unperturbed metal linking the layer b and the surface layer, 1, $\widehat{T}_{ab}(k_{\parallel})$ is a hopping matrix connecting layers a and b , and $\widehat{\rho}_{00}(E)$ is the density of states on the last atom of the tip (0), considered for simplicity to be the only tip active atom for tunneling (this is a good approximation, since usually BEEM experiments are performed under conditions where the tip-metal distance is large). The trace denotes a summation over the orbitals forming the chosen basis.

Step 3 of our scheme involves computing the transmission coefficient for the two-dimensional interface. Applying a surface Green's function matching formalism [13] in the neighbourhood of the \overline{M} point (corresponding to projections of X and L points in the 3D fcc Brillouin zone [2]), we obtain a transmission coefficient $T(E, k_{\parallel})$ [12] that can be used in k -space to give the injected current in the semiconductor

$$I(V) = \int_{E_F+eV_0}^{E_F+eV} dE \int_{1\text{stBZ}} dk_{\parallel} J_{c-1,c}(E, k_{\parallel}) \times T(E, k_{\parallel}), \quad (4)$$

where c refers to the metal layer at the interface, and V_0 is the Schottky barrier height (assumed to be 0.86 eV); note that the transmission coefficient is zero outside the ellipsoids allowed by energy conservation (see fig. 1). The integral inside the first Brillouin zone is performed summing over a dense grid of special points [14].

In previous publications we have discussed how the propagation of electrons in the gold periodic lattice results in focused beams and narrow Kossel-like lines in real space, with a 3-fold symmetry associated to the (111) direction of an fcc crystal [6, 10, 12]. These lines have typical widths of around 3-4 atomic distances, explaining the nanometric resolution of the BEEM technique even in deeply buried interfaces. These results also show how the Bloch wave is formed after propagation by more than four or five layers, forbidding the propagation of electrons in gap directions over longer distances. We believe that our results are convincing enough to answer a question nowadays found in the literature related to Monte Carlo simulations: is it realistic to assume that electrons can propagate 20 or 30 Å as free particles along the forbidden Au(111) directions? We conclude that this is an unphysical

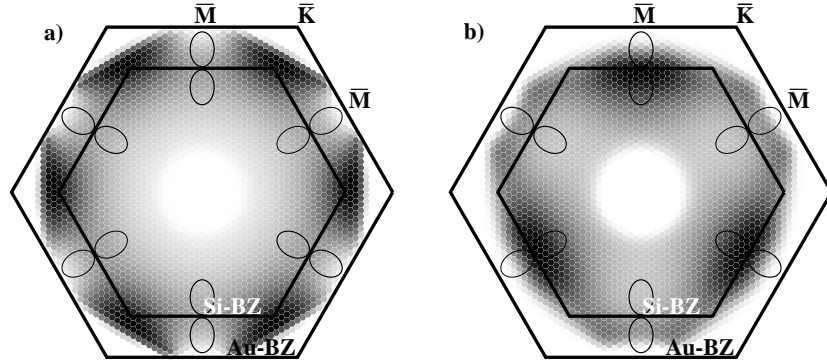


Fig. 1. – a) k -space current distribution for Au(111) inside the coherence region (5th atomic layer) ($V = 1$ eV, $\eta = 0.1$ eV); b) same as a), but outside the coherence region (30th atomic layer). Dark regions correspond to higher intensities. The Si BZ (small) and the Au BZ (large) are shown together with the ellipses where the Si conduction band minima project (notice that the outer ellipses appear after the corresponding remapping).

scenario because of the strong deflection exerted by the lattice on electrons traveling in these directions.

However, in this work we shall focus on our results in 2D reciprocal space, and their influence on the $I(V)$ curves. An important feature observed in k_{\parallel} -space is a change in the symmetry of the current distributions when going from thin to thick layers. The expected symmetry for a quantum-mechanical calculation is related to the projected density of states [15]. It is six-fold in (111) fcc planes, because of the equal contribution of $+\vec{k}$ and $-\vec{k}$ states. This is indeed the case for an arbitrarily small imaginary part (η) added to the energy, but as commented above, η can be interpreted in terms of a complex self-energy arising from inelastic events defining a coherence region of the order of λ_{att} . Beyond that region inelastic processes become important, and intensities rather than amplitudes add to give the final wavefield. This takes us from a quantum-mechanical picture (six-fold) to a semi-classical one (three-fold), as can be seen comparing fig. 1a), inside the coherence region, to fig. 1b), where the current distribution is computed in a layer outside that area. The three-fold symmetry is progressively built up as a function of metal thickness, and can be understood in terms of our previous analysis [6]: the symmetry of the wavefield in the semiclassical limit is related to the Fermi surface, reflecting the three-fold symmetry of the crystal. Therefore, this is a new example of how a quantum system, under the influence of friction, becomes gradually classical by a decoherence process [16]. In addition, it is seen how the current in k -space deviates for these thick layers from a simple density of states calculation [15], concentrating around the directions predicted by the semiclassical analysis (fig. 1b)) [6,10]. The difference observed in 2D reciprocal space between the quantum and semiclassical regime does not significantly affect the beams in real space (where the symmetry must always be three-fold), but could in principle affect the $I(V)$ current injected through the projected ellipses into the semiconductor. However, because of the gradual crossover seen from one regime to the other, we do not expect dramatic effects, unless one could experimentally break the time-reversal symmetry suddenly (*e.g.*, by application of a magnetic field), or could selectively block the current injected in some of the six equivalent ellipsoids. In those cases, a sudden jump between a semiclassical regime and a quantum one should be observable. It should be noted that band structure effects result in k -space current with enough k_{\parallel} to have the electrons injected into the outer conduction band

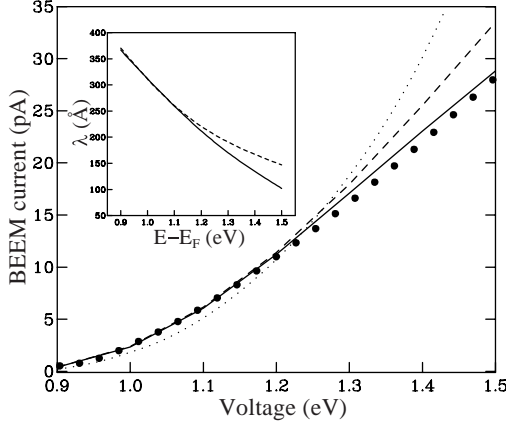


Fig. 2

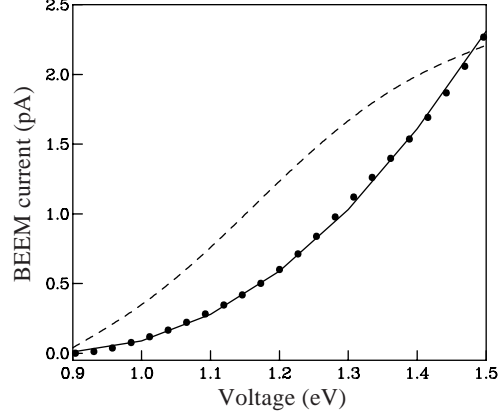


Fig. 3

Fig. 2. – Theoretical $I(V)$ curves for Au/Si(111), $d = 75 \text{ \AA}$. Different curves are: solid circles: experimental values from ref. [17]; dotted line: ballistic theory; dashed line: theory using an RPA approximation for $\lambda_{\text{att}}(E)$ (see eq. (5) with $\lambda^0 = 260 \text{ \AA}(\text{eV})^2$ ($\lambda(E)$ -RPA is displayed in the inset as a dashed line); solid line: theory using a λ_{att} modified over the RPA as described in the text ($\lambda(E)$ modified is displayed in the inset as a solid line).

Fig. 3. – Theoretical $I(V)$ curves for Au/Si(111), $d = 300 \text{ \AA}$ (solid circles: experimental values from ref. [17]); dashed line: RPA with $\lambda^0 = 175 \text{ \AA}(\text{eV})^2$; solid line: RPA with $\lambda_{\text{att}} = 125 \text{ \AA}$ for all E .

minima of Si (the central one is forbidden because of the gap in that direction), and explains the long-standing puzzle of why the threshold on Au/Si(111) and Au/Si(100) is nearly the same: our calculations show how the similar results obtained for both interfaces are related to these nontrivial distributions in k -space, after the appropriate folding of the gold Brillouin zone inside the silicon one is performed [12].

Next, we compute theoretical $I(V)$ curves from eq. (2). A quantitative comparison with BEES experiments [17] will then allow us to discuss also the electronic mean free paths. First of all, we try the hypothesis of ballistic electrons. On intuitive grounds this should suffice for low temperature, low voltages, and very thin layers. In fig. 2 we compare experimental results for Au/Si(111) at $T = 77 \text{ K}$, $d = 75 \text{ \AA}$ [17] with a pure ballistic calculation (η very small and injection at first attempt). It is clear from these results that, *without using any adjustable parameter*, the onset is reasonably explained by a purely ballistic theory that *uses the right current distributions in k -space*. Therefore, we are able to give a reasonable explanation of the experiment for voltages near the threshold, but it is also noticed in fig. 2 that data beyond $V = 1.2 \text{ eV}$ can only be consistently interpreted by assuming an attenuated wave. To introduce an attenuation mechanism, people have considered three major sources of damping: electron-electron, electron-phonon and electron-defect interaction. As the electron-phonon contributions are greatly reduced at 77 K , we first consider a $\lambda_{\text{att}}(E)$ dominated by the electron-electron interaction. Within an RPA approximation for a free-electron gas with a density representing gold ($r_s = 3.01$), we obtain

$$\lambda_{\text{att}}(E) = \lambda^0 \frac{E/E_F}{(E - E_F)^2}, \quad (5)$$

with $\lambda^0 = 260 \text{ \AA}(\text{eV})^2$. Results considering multiple reflections [17] between the surface and

the interface through a *specular* model are presented in fig. 2, where an excellent agreement is seen again up to 1.2 eV. Beyond that voltage, a reduction in the attenuation length by about 20% on average is required to bring experimental and theoretical intensities close together. The modified $\lambda_{\text{att}}(E)$ is displayed in the inset of fig. 2 (continuous line) together with the pure RPA one (dashed line) for comparison. The reduction with respect to the first-principles RPA approximation might be understood as representing either band structure or impurity effects in the effective electron-electron interaction, and further work is currently in progress to try to understand better its physical origin. The good agreement obtained for low voltages is remarkable, where λ_{att} changes quickly with energy following an RPA-like behaviour. This is at variance with E -space Monte Carlo simulations whereby a smoother dependence of λ_{att} on energy was found [17]. Our results suggest, however, that for thin films and low voltages, the main source of damping is the electron-electron interaction that is well described within a RPA approach.

However, a different example of BEES data, where a pure ballistic theory is not sufficient even near the threshold, is afforded by the case of thick layers (see fig. 3). In this case we notice that if we use an RPA-like energy dependence for λ_{att} , we find both a discrepancy in magnitude and a different voltage dependence for $I(V)$ (as seen in the different slopes). If we choose a different λ^0 in the RPA expression to get the right magnitude, we still would observe a serious discrepancy with the experiment (*e.g.*, see fig. 3 where λ^0 has been reduced to $175 \text{ \AA}(\text{eV})^2$). Because all the other elements in the theory that might be responsible for the discrepancy ($J(E)$ and $T(E)$ in formula (4)) are calculated from first principles, we take this as a serious indication of a different dependence of $\lambda_{\text{att}}(E)$ on energy. A possible physical origin for this effect is the likely presence of defects (*e.g.*, vacancies) [18]. The natural choice for this scenario is an energy-independent attenuation length in the Green function. With this assumption we obtain an excellent agreement with the experiment ($T = 77 \text{ K}$, $d = 300 \text{ \AA}$ [17]) for $\lambda_{\text{att}} = 125 \text{ \AA}$, as seen by the solid line in fig. 3. This value is in reasonable agreement with attenuation lengths derived by different groups in films of similar thickness [17, 18], but a different theoretical approach, more appropriate to analyze the effect of impurities on the BEEM current (like k -space Monte Carlo simulation) should be used to further clarify this point on thick layers.

In conclusion, we have introduced a Green's function formalism that in the ballistic limit is an *ab initio* approach to BEEM. The particular k_{\parallel} -space current distributions determined by band structure effects are the main result of our analysis and crucial for a quantitative comparison with experimental BEEM data. Inelastic effects have also been approximately included by use of an imaginary self-energy. This single quantity is fitted to the experiments to explain a number of spectroscopic data on the Au/Si interface.

We are indebted to Prof. K. HEINZ for his support. KR is grateful for financial support from SFB292 (Germany). We acknowledge financial support from the Spanish CICYT under contracts number PB97-1224 and PB97-0028.

REFERENCES

- [1] KAISER W. J. and BELL L. D., *Phys. Rev. Lett.*, **60** (1988) 1406; BELL L. D. and KAISER W. J., *Phys. Rev. Lett.*, **61** (1988) 2368.
- [2] For comprehensive reviews see PRIETSCH M., *Phys. Rep.*, **253** (1995) 164; BELL L. D. and KAISER W. J., *Annu. Rev. Mater. Sci.*, **26** (1996) 189.
- [3] LUDEKE R., *Phys. Rev. Lett.*, **70** (1993) 214.

- [4] MILLIKEN A. M., MANION S. J., KAISER W. J., BELL L. D. and HECHT M. H., *Phys. Rev. B*, **46** (1992) 12826.
- [5] SCHOWALTER L. J. and LEE E. Y., *Phys. Rev. B*, **43** (1991) 9308.
- [6] GARCIA-VIDAL F. J., DE ANDRES P. L. and FLORES F., *Phys. Rev. Lett.*, **76** (1996) 807.
- [7] SLATER J. C. and KOSTER G. F., *Phys. Rev.*, **94** (1954) 1498.
- [8] PAPACONSTANTOPOULOS D. A., *Handbook of the Band Structure of Elemental Solids* (Plenum, New York) 1986.
- [9] KELDysh L. V., *Sov. Phys. JETP*, **20** (1965) 1018.
- [10] DE ANDRES P. L., GARCIA-VIDAL F. J., SESTOVIC D. and FLORES F., *Phys. Scr.*, **T66** (1996) 277.
- [11] GUINEA F., TEJEDOR C., FLORES F. and LOUIS E., *Phys. Rev. B*, **28** (1983) 4397.
- [12] DE ANDRES P. L., REUTER K., GARCIA-VIDAL F. J., SESTOVIC D. and FLORES F., *Appl. Surf. Sci.*, **123/124** (1998) 199; cond-mat/9710091.
- [13] GARCIA-MOLINER F. and FLORES F., *Introduction to the Theory of Solid Surfaces* (Cambridge University Press, Cambridge) 1979.
- [14] RAMIREZ R. and BÖHM M. C., *Int. J. Quantum Chem.*, **30** (1986) 391.
- [15] STILES M. D. and HAMANN D. R., *Phys. Rev. Lett.*, **66** (1991) 3179.
- [16] ZUREK W. H., *Phys. Today*, **44** (Oct. 1991) 36.
- [17] BELL L. D., *Phys. Rev. Lett.*, **77** (1996) 3893.
- [18] VENTRICE C. A. jr., LABELLA V. P., RAMASWAMY G., YU H. P. and SCHOWALTER L. J., *Phys. Rev. B*, **53** (1996) 3952.